Algebraic filters for filtered backprojection

Plantagie, L.

7

THE ACCURACY OF FBP WITH RECENTLY INTRODUCED FILTERS: A COMPARISON

7.1 INTRODUCTION

The field of *Computerized tomography* (CT) focuses on reconstructing an image of a scanned object from its projections. Projection data are obtained using a scanning device, for example using X-rays (CT-scanning) or electrons (electron microscopy). The size of objects that can be scanned by tomography varies from nanometers in electron tomography to kilometers in seismic tomography [1–4].

In many tomography applications, such as medical and industrial imaging, finding an exact reconstruction is not possible due to the size of the reconstruction problem and due to inconsistent projection data. Therefore, many algorithms have been developed that approximate the scanned object. Two common categories of such methods are the algebraic reconstruction methods and the analytical reconstruction methods.

The *algebraic reconstruction methods* (ARMs) use a discrete representation of the tomographic reconstruction problem. This approach often involves iterative reconstruction techniques to solve the system of linear equations. Examples of these methods are the Kaczmarz method which is also known as the algebraic reconstruction technique (ART) and the simultaneous iterative reconstruction technique (SIRT). Also expectation maximization (EM) is a well-known iterative recon-

The author would like to acknowledge Dr. D.M. Pelt from the Centrum Wiskunde & Informatica, Amsterdam, The Netherlands, for developing the software that was used to generate the reconstructions for the experiments in this chapter and for his useful textual comments.

struction method [5, 6]. Algebraic reconstruction methods are well-suited for incorporating certain types of prior knowledge. These methods are preferred for limited-data problems, for example if only projections from few angles are available, or if the projections have a limited angular range. A disadvantage of algebraic methods is their high computational burden, which can become a bottleneck if large objects, or a large number of objects, have to be reconstructed in a short period of time.

The *analytical reconstruction methods* are based on a continuous representation of the tomographic reconstruction problem. The *Filtered Backprojection* algorithm (FBP) is a commonly used reconstruction method in CT imaging. It is a computationally fast reconstruction method, since it only requires a filtering step followed by a backprojection step. For low-noise projection data with a substantial number of equiangularly distributed projection angles, FBP is known to produce accurate reconstructions.

Due to the computational efficiency of FBP, extensive efforts have been made to improve the quality of its reconstructions for situations where FBP is known to produce poor quality reconstructions. This reconstruction quality depends strongly on the filters that are used in the FBP algorithm. Choosing the optimal filter for a particular reconstruction problem is not straightforward and often some standard variation on the Ramp filter is used. Many methods have recently been published to create filters for FBP. In this chapter we will compare methods that can be used in 2D parallel-beam tomography.

New filters can be obtained from theoretical derivations, as shown by Zeng [7]. Other methods, such as OFBP [8] and AF-FBP [9], create new filters using information from algebraic reconstruction methods and thereby incorporating the geometry of the reconstruction problem in the filters. Applying neural networks is another approach to obtaining filters for FBP, as shown by Pelt and Batenburg [10]. Pelt and Batenburg also introduce the method MR-FBP [11], where the filter depends on the measured projection data.

Also in the field of tomosynthesis, creating better filters for FBP has been a topic of interest. An example is OFBP, which was already mentioned above. Also Godfrey et al. [12] and Nielsen et al. [13] have recently introduced new filter methods for FBP. Since these algorithms cannot be translated into parallel-beam tomography, as opposed to OFBP, they will not be included in this chapter.

In this chapter, we will provide an overview of recently proposed methods to compute filters for the FBP algorithm. While the original descriptions of these methods are quite diverse, we formulate a common framework in which each of these methods can be expressed in a straightforward way. After an introduction to the various methods covered in this chapter, we will provide an analysis of the characteristic properties of each method. An illustration of the results obtained from the various filter methods is subsequently provided through a series of simulation experiments. We conclude this chapter with discussion and conclusions.

7.2 METHODS

In this section, we first describe the geometry that will be used in this chapter and the FBP method with standard filters. Then we give a short description of the methods that will be compared throughout this chapter.

We consider a parallel-beam geometry with a monochromatic X-ray source rotating in a circular trajectory around the object. The object is represented as a function $f : \mathbb{R}^2 \to \mathbb{R}$. We denote the set of projection angles by Θ with $N_\Theta = |\Theta|$, and the set of detector bins by T with $N_T = |T|$. Define $N_{T\Theta} = N_T N_\Theta$. Furthermore we denote the projections by $\mathbf{p} \in \mathbb{R}^{N_{T\Theta}}$.

We assume that the measured projections are related to the object f by the continuous Radon transform, given in Eq. (7.1).

$$p(\theta, t) = (\mathcal{R}f)(\theta, t) = \int_{-\infty}^{\infty} f(t\cos\theta - s\sin\theta, t\sin\theta + s\cos\theta)\, ds \tag{7.1}$$

So, for each projection angle $\theta \in \Theta$, we obtain the value of the Radon transform for a discrete set of detector coordinates T. The *reconstruction problem* then consists of recovering the function f from this set of measurements.

In algebraic methods, the domain of f is discretized as a discrete (typically square) set of $N \times N$ pixels, forming a vector of N^2 pixel values. Similarly, the measured projections are represented by a vector of

size $N_{T\Theta}$. This leads to the following discretized version of the reconstruction problem:

$$\boldsymbol{W}\mathbf{x} = \mathbf{p}. \tag{7.2}$$

In this system of linear equations, the vector $\mathbf{x}$ represents the unknown object, the vector $\mathbf{p}$ represents the combined projection data for all angles, and the projection matrix $\boldsymbol{W}$ models a discretization of the Radon transform, defining the relationship between $\mathbf{x}$ and $\mathbf{p}$.

This chapter deals with *filtered backprojection* methods, which can all be written as

$$\mathbf{u} = \boldsymbol{W}^T\mathbf{H}\mathbf{p}, \tag{7.3}$$

where $\mathbf{u} \in \mathbb{R}^{N^2}$ denotes a vector containing the $N \times N$-reconstruction, $\boldsymbol{W}^T$ denotes the *transpose* of the projection matrix (also known as the backprojection operator), and $\mathbf{H} \in \mathbb{R}^{N_{T\Theta} \times N_{T\Theta}}$ denotes some filter matrix. The particular choice of the filter matrix $\mathbf{H}$ defines the reconstruction algorithm. In the following subsections we will introduce a series of filtered backprojection methods that have been proposed in the literature.

7.2.1 *FBP*

We first briefly comment on the FBP method itself. We recall that the Radon transform in Eq. (7.1) has an exact inversion formula given by Eq. (7.4).

$$f(x, y) = \int_0^\pi \int_{-\infty}^{\infty} p(\theta, \tau) g(\theta, t - \tau)\, d\tau d\theta, \tag{7.4}$$

where $g : \mathbb{R}^2 \to \mathbb{R}$ is the inverse Fourier transform of the *Ramp filter* $G(\theta, q) = |q|$.

The FBP method is obtained by discretizing Eq. (7.4), as follows:

$$f(x, y) = \sum_{\theta \in \Theta} \sum_{\tau \in T} p_{\theta\tau} g(\theta, \tau - x\cos\theta - y\sin\theta). \tag{7.5}$$

Hence FBP can be written in the form of Eq. (7.3), where $\mathbf{H}$ is defined by the filters g. The actual filter that is used in FBP does not have to be

the Ramp filter. In fact, each of the methods that we will cover in this chapter uses a different filter g.

7.2.2 *Standard filters for FBP*

There are several common filters for FBP, which will be called *standard filters* here. These filters are variations of the Ramp filter. The Ramp filter itself is not commonly used, since it amplifies the noise in the high frequencies, resulting in a poor reconstruction quality. Therefore, frequency windows are applied to the Ramp filter.

A well-known filter was proposed by Ramachandran and Lakshminarayanan. It uses a simple windowing function, as shown in Eq. (7.6) [2, 14]. We refer to this filter as the *Ram-Lak* filter.

$$G(\theta, q) = |q| \operatorname{rect}(q). \tag{7.6}$$

Other, more smooth filter functions are the *Cosine* filter and the *Hann* filter, see Eq. (7.7) and Eq. (7.8) respectively.

$$G(\theta, q) = |q| \operatorname{rect}(q) \cos(\pi q/2), \tag{7.7}$$

$$G(\theta, q) = |q| \operatorname{rect}(q) (0.5 - 0.5 \cos(2\pi q)). \tag{7.8}$$

The latter two functions aim at smoothening the edges of the Ram-Lak filter. The advantage of the Cosine and Hann filter is that they reduce image noise. A disadvantage is that they do not preserve edges in the image.

A major advantage of the FBP method with such a standard filter is its computational efficiency. The complexity of the filtering step in the Fourier space is $\mathcal{O}(N_{T\Theta} \log N_T)$ and a backprojection operation is $\mathcal{O}(N_T N^2)$. The standard filters are independent of both the object to be scanned and the geometry that is used, including the number of projection angles and the size of the reconstruction grid. A drawback is that no prior knowledge can be incorporated. Furthermore, FBP with standard filters is known to perform poorly in case of a missing wedge or limited number of projection angles.

7.2.3 *MR-FBP*

The method minimal residual filtered backprojection (MR-FBP) is proposed by Pelt and Batenburg (2014). It is designed for limited-data problems and it aims at finding the filter that minimizes the projection error of the resulting reconstruction, i.e. the difference between the forward projection of the reconstruction and the projection data $\mathbf{p}$.

FBP consists of a filtering step, which is a convolution of the projection data $\mathbf{p}$ by some filter, followed by a backprojection. As argued in [11], FBP can also be written as a convolution of some filter $\mathbf{h}$ by $\mathbf{p}$, followed by a backprojection operation, see Eq. (7.9).

$$\mathrm{FBP}_{\mathbf{h}}(\mathbf{p}) = \boldsymbol{W}^{\mathsf{T}} \mathbf{C}_{\mathbf{p}} \mathbf{h}, \tag{7.9}$$

where $\mathrm{FBP}_{\mathbf{h}}$ denotes FBP with the filter $\mathbf{h}$ applied, $\boldsymbol{W}^{\mathsf{T}}$ is the backprojection, and the matrix $\mathbf{C}_{\mathbf{p}}$ is the convolution by $\mathbf{p}$. The filter $\mathbf{h}$ is chosen such that it minimizes the squared difference between the forward projection of the reconstruction and the measured projection data.

$$\mathbf{h}^* = \operatorname*{argmin}_{\mathbf{h}} [\mathbf{p} - \boldsymbol{W}\boldsymbol{W}^{\mathsf{T}} \mathbf{C}_{\mathbf{p}} \mathbf{h}]^2. \tag{7.10}$$

Exponential binning is used to reduce the number of unknowns for the filter $\mathbf{h}$ [11]. The resulting MR-FBP algorithm requires the computation of $\mathcal{O}(\log N_T)$ projection operations and the total computation time is $\mathcal{O}(N_\Theta N^2 \log N_T + N_{T\Theta} [\log N_T]^2)$ for $N_T \approx N$.

The filter $\mathbf{h}^*$ is designed to minimize the residual in Eq. (7.10). It determines the filter as part of the reconstruction algorithm, since the optimal filter depends on both the object to be scanned and the scanning geometry. Therefore, the geometry can be altered during the experiments, as opposed to some other reconstruction methods discussed in this chapter. It is also possible for this method to incorporate prior knowledge for example by adding a regularization term to Eq. (7.10). Determining the filter is relatively fast and various scanning geometries can be used.

A disadvantage of MR-FBP is that it is less suited for creating large numbers of reconstructions with the same geometry, because the filter depends on the measured projection data. The filter therefore changes for every scanned object.

7.2.4 *AF-FBP*

Filters for FBP can also be created using a linear algebraic reconstruction method (ARM). In [9], Batenburg and Plantagie introduce the method algebraic filter - filtered backprojection (AF-FBP). They use the simultaneous iterative reconstruction technique (SIRT) to demonstrate the characteristics of this method. We will follow this approach here.

For any linear algebraic reconstruction method, there exists a transformation matrix $\mathbf{R} \in \mathbb{R}^{N^2 \times N_{T\Theta}}$ such that $\mathbf{u} = \mathbf{Rp}$. For some pixel c of the reconstruction grid, denoted by (x_c, y_c), define its projection onto the detector by $t_c^{(\theta)} = x_c \cos\theta + y_c \sin\theta$ for $\theta \in \Theta$. Furthermore, let $\mathbf{r}^{(c)}$ denote the cth row of $\mathbf{R}$ and $r_{\theta\tau}^{(c)}$ the entry of this row corresponding to angle θ and detector element $\tau \in T$. It is shown in [9] that there exists a function $h^{(c)}$ such that

$$u_c = \sum_{\theta\in\Theta} \sum_{\tau\in T} p_{\theta\tau} h^{(c)}(\theta, \tau - t_c^{(\theta)}). \tag{7.11}$$

When c is chosen such that it is the central pixel of the reconstruction grid, then $h^{(c)}$ can be expressed as $\mathbf{R}$ applied to a set of unit vectors $e_{\theta\tau}$ with value 1 at position (θ, τ) and value 0 otherwise, see Eq. (7.12).

$$h_{\theta\tau}^{(c)} = [\mathbf{R}\boldsymbol{e}_{\theta\tau}]_c, \quad \forall\theta \in \Theta, \tau \in T. \tag{7.12}$$

This angle dependent filter is then applied to obtain all image pixels of the reconstruction. As shown in [9], the characteristics of these reconstructions resemble those of the linear ARM that was used to create the filters. The reconstruction time is however significantly reduced compared to that of the ARM, since FBP can be used for the reconstruction. This is advantageous in situations with only few projection angles or limited projection range, where an ARM in general gives more accurate reconstructions than FBP with standard filters. When the computational burden of ARMs prevents the use of such an ARM, AF-FBP could be a good alternative. Another advantage of AF-FBP is that certain types of prior knowledge can be incorporated when creating the filters.

A disadvantage of AF-FBP is the time that is needed to create its filters. It takes $\mathcal{O}(N_{T\Theta})$ ARM reconstructions to obtain this filter. Howe-

ver, since the filter is object independent, these calculations need only be executed once for a given geometry. Furthermore, not all ARMs are suitable for AF-FBP, since only linear ARMs can be used. The geometry is currently limited to 2D parallel beam. Several parameters need to be set in advance, such as the pixel c and the number of iterations k. Also a relaxation parameter ω needs to be chosen, which is contained in SIRT.

7.2.5 *Zeng*

In [7], Zeng uses the algebraic Landweber algorithm to obtain a filter for FBP. The Landweber algorithm is an iterative algebraic reconstruction method that solves the system of linear equations $\boldsymbol{W}\mathbf{x} = \mathbf{p}$ to obtain the minimum least squares solution. It is equivalent to SIRT that is used by AF-FBP. The kth iteration step of the Landweber algorithm is given by Eq. (7.13).

$$\mathbf{x}^{(k+1)} = \mathbf{x}^{(k)} + \omega \boldsymbol{W}^{T}(\mathbf{p} - \boldsymbol{W}\mathbf{x}^{(k)}), \tag{7.13}$$

where ω is a relaxation parameter. Zeng describes a method to obtain a filter in the frequency domain based on this Landweber algorithm. The filter can be used in the FBP method.

The first step to deduce the formula for this filter, is to rewrite Eq. (7.13) into the form in Eq. (7.14), where $\mathbf{x}^{(0)}$ is assumed to equal zero and k is finite.

$$\mathbf{x}^{(k)} = (\boldsymbol{W}^{T}\boldsymbol{W})^{-1}[\mathbf{I} - (\mathbf{I} - \omega \boldsymbol{W}^{T}\boldsymbol{W})^{k}]\boldsymbol{W}^{T}\mathbf{p}, \tag{7.14}$$

where $\mathbf{I}$ denotes the identity matrix.

It is shown by Zeng that the impulse-response of the matrix $\boldsymbol{W}^{T}\boldsymbol{W}$, determined in the central region of the reconstruction grid, behaves approximately as $1/r$. This means that if we move away from the central pixel along radial lines, the intensity observed decays as $1/r$. Furthermore, the 1D Ramp filter is a good approximation of the operation $(\boldsymbol{W}^{T}\boldsymbol{W})^{-1}$. Hence the filter in 1D Fourier space is given by Eq. (7.15).

$$H_k(\nu_t) = |\nu_t|\Big[1 - \Big(1 - \frac{\omega}{|\nu_t|}\Big)^{k}\Big], \tag{7.15}$$

where ν_t denotes the spatial frequency with respect to the detector.

When we compare the filter in Eq. (7.15) with the general form in Eq. (7.3), we see that the filter $\mathbf{H}$ is given by a 1D Fourier transform of $\mathbf{p}$ followed by applying the windowed ramp filter H_k and a 1D inverse Fourier transform of this filtered data.

An advantage of this method is that the computational burden to obtain the filter is low. Furthermore, the filter can be obtained for a variety of geometries and is independent of the object to be scanned.

This method is specifically designed to approximate the Landweber algorithm. It is therefore not directly applicable to other algebraic reconstruction methods. It requires the start solution $\mathbf{x}^{(0)}$ to be equal to zero and the number of iterations k has to be chosen in advance. The parameter ω needs to be chosen appropriately, since a value exceeding $2/\sigma_{max}$, with σ_{max} the largest singular value of $\boldsymbol{W}^T\boldsymbol{W}$, results in a diverging algorithm, while the rate of convergence decreases with a decreasing ω.

7.2.6 *OFBP*

Filters for FBP can also be created based on the impulse response of an algebraic reconstruction algorithm, as observed by scanning a very thin object on the detector. The method optimized filtered backprojection (OFBP) is an example of such a method. It is described by Kunze et al. in 2007 for breast tomosynthesis, with typically few projection angles and a limited angular range[8].

The iterative reconstruction method SIRT is used to derive a method to obtain filters for FBP. Kunze et al. derive an iterative method called *corrected projections simultaneous iterative reconstruction techniques* (P-SIRT) which has its update step in the projection space followed by a backprojection, see Eq. (7.16).

$$\begin{aligned}\mathbf{p}^{(k+1)} &= \mathbf{p}^{(k)} + \mathbf{p} - \boldsymbol{W}\omega\boldsymbol{W}^T\mathbf{p}^{(k)},\\ \mathbf{u}^{(k+1)} &= \omega\boldsymbol{W}^T\mathbf{p}^{(k+1)},\end{aligned} \tag{7.16}$$

where ω is a relaxation parameter. The initial parameter $\mathbf{p}^{(0)}$ equals the measured projection data $\mathbf{p}$.

In the limit case $k \to \infty$, a reconstruction of P-SIRT is given by Eq. (7.17).

$$\mathbf{u}^{(\infty)} = \omega \boldsymbol{W}^{\mathsf{T}} (\boldsymbol{W} \omega \boldsymbol{W}^{\mathsf{T}})^{-1} \mathbf{p}, \tag{7.17}$$

The matrix $\mathbf{H} = \omega(\boldsymbol{W}\omega\boldsymbol{W}^{\mathsf{T}})^{-1}$ acts as a filter on the projection data.

Exact inversion of this matrix is difficult to perform due to the large scale of the problem. Kunze et al. approximate this inversion by simulating Dirac-line-functions using thin wires to determine the impulse responses. These impulse responses are then used as the corresponding angle-dependent filters for FBP.

Kunze et al. use three thin wires to determine three impulse responses. These impulse responses are then averaged to obtain the filters. The impulse response is assumed to have finite support and to be shift invariant within a projection angle. The distance between the wires should be large enough to avoid overlapping of the impulse responses. It is shown in [8] that the impulse responses for the top, middle and end of a wire are very similar, hence no averaging is needed in the direction of the wire. The impulse response corresponding to the middle of the wire is used for the filters. It is furthermore assumed that the filters created using these wires are independent for each projection angle.

An advantage of this method is that the computational burden to create the filters is low. Furthermore, since the filters are object independent, the filters need only be determined once for a given geometry and scanning device. With this method it is possible to incorporate prior knowledge when determining the filters.

A disadvantage of the method is that it is designed to approximate P-SIRT only. It is not possible to create filters with this method that can be used to approximate other algebraic reconstruction methods. Furthermore, as opposed to the other methods presented here, a specific object needs to be scanned to be able to determine the impulse responses, i.e. the three thin wires. As a result, the filters depend on the geometry and on the scanning device that is used to create the filters. Parameters that need to be chosen are the number of iterations, the thickness and position of the wires, the supersampling and interpolations that need to be used.

7.2.7 *lNN-FBP*

A different approach for solving the CT reconstruction problems is by using neural networks. In [10] the neural network filtered backprojection method (NN-FBP) is introduced. The NN-FBP method consists of two stages: a *training stage* and a *reconstruction stage*. For the training stage, a series of high quality images of typical objects is required, along with their projections. It is important that these images are representative for the objects that will be reconstructed later on, in the reconstruction stage. In the training stage, a *supervised learning algorithm* is employed, to derive a set of filters such that the reconstructed pixel values for the training set are as similar as possible to the high quality test images. This learning algorithm is based on neural network theory. More concrete, the neural network is modeled as a multilayer perceptron. It consists of a layer of input nodes z, a weight matrix $\hat{\boldsymbol{W}}$, a layer of hidden nodes $\hat{\mathbf{h}}$, an activation function σ that is applied to the output of each node, and a second weight matrix $\mathbf{Q}$. With appropriate choices of the variables, this network can be written as a weighted sum of Filtered Backprojections. As a full description of the network model is outside the scope of our current description, we refer to [10] for the exact details. By reducing the number of hidden nodes in the network to one, and choosing a linear activation function σ equal to the identity function, the neural network can even be written as a single filtered backprojection operation as shown in Eq. (7.18). We refer to this method as linear NN-FBP (lNN-FBP).

$$n_{\mathbf{Q},\hat{\mathbf{H}}}(z) = q_0 \mathrm{FBP}_{\hat{\mathbf{h}}_0}(x,y) = [\hat{\boldsymbol{W}}^T q_0 \hat{\mathbf{h}}_0 \mathbf{p}]_{(x,y)}, \tag{7.18}$$

where the function $n_{\mathbf{Q},\hat{\mathbf{H}}}(z)$ defines the value of a single reconstructed pixel (x,y), based on the network parameters $\mathbf{Q}$ and $\hat{\mathbf{H}}$, and on the input projection data z. The input values for z are derived from the projection data after a translation and reflection operation.

Pelt and Batenburg use an independent validation set during the training phase to avoid overfitting. After obtaining the optimal values q_0^* and $\hat{\mathbf{h}}_0^*$ for q_0 and $\hat{\mathbf{h}}_0$ respectively, and due to the shift invariance of FBP, a reconstruction with lNN-FBP is obtained from a single FBP with filter $\mathbf{h} = q_0^* \hat{\mathbf{h}}_0^*$ applied to the projection data. This filter is angle independent. The computational complexity of the reconstruction part of lNN-FBP with one hidden node equals $\mathcal{O}(N_\Theta N^2)$.

For lNN-FBP a large training set of images is needed. If there is prior knowledge available of the object to be scanned, then this can be incorporated by the choice of this training set. An additional advantage of this method is that the optimal filters need only be computed once for a given training set. Furthermore, since FBP is shift-invariant, the filter calculation need not be repeated for every pixel of the reconstruction. The method is described here for a 2D scanning geometry. It is however also suitable for extension to 3D scanning geometries.

A drawback of the method is that the object to be scanned needs to be close enough to the training set, otherwise the parameters $\mathbf{Q}$ and $\hat{\mathbf{H}}$ are no longer accurate to minimize the squared difference between the reconstruction and the original object. Furthermore, the quality of the reconstructions depends on several decisions which have to made in advance. These include the size of the training set and the method to obtain correct outputs (i.e. FBP with a standard filter or an algebraic reconstruction method with a high number of projection angles). It is furthermore known from literature that linear NN-FBP is less accurate than a normal NN-FBP with multiple nodes and with a nonlinear activation function σ.

7.2.8 *Characteristics*

We conclude this section with a brief overview of the main characteristics of the reconstruction methods that have been introduced above.

The first characteristic that we consider is the ability to handle few projection angles, see also Table 7.1. The standard filters for FBP and the method of Zeng are known to produce poor quality reconstructions for these datasets, while MR-FBP, AF-FBP, OFBP and lNN-FBP can handle this input much better since they create filters based on an explicit model of the projection angles that are actually available.

The ability to handle noisy projection data varies amongst the different filter methods. The Ram-Lak filter amplifies high frequencies and thus noise. The Cosine and Hann filters do not amplify these high frequencies and can handle noisy data better. MR-FBP, AF-FBP, OFBP and lNN-FBP perform better in reducing noise than FBP with standard filters. According to its inventor, the filter of Zeng depends on the index k which is the number of iterations in the Landweber method. For low k the noise is reduced while for high k the resolution increases and

Method	FBP-RL	FBP-Cos	FBP-Hann	MR-FBP	AF-FBP	Zeng	OFBP	lNN-FBP
Handling few projection angles	-	-	-	+	+	-	+	+
Noise reduction	--	-	-	+	+	+/-	+	+
Prior knowledge	-	-	-	+/-	+/-	-	+/-	+
Variable geometry	v	v	v	v	x	v	x	x
Preprocessing time	+	+	+	+	-	+	+/-	-
Reconstruction time	+	+	+	+/-	+	+	+	+
Requiring a training set	x	x	x	x	x	x	x	v
Requiring a phantom for the filter	x	x	x	x	x	x	v	x
Filter depends on the object	x	x	x	v	x	x	x	x

Table 7.1: Characteristics of the different filtering methods; v = yes, x = no, - (——) = (very) incapable or slow, + = capable or fast, +/- = intermediate.

the noise is amplified. The results of OFBP and AF-FBP also depend on the parameter k.

The methods MR-FBP, AF-FBP, OFBP and lNN-FBP are suitable to incorporate some types of prior knowledge of the scanned object by using an L2 regularization. For lNN-FBP more object specific information can be incorporated in the training stage.

The geometry can be chosen freely for FBP with standard filters, MR-FBP and Zeng. For the other methods the filters are created based on a certain geometry. When the number of projection angles or the size of the detector or reconstruction grid changes, new filters should be calculated based on this new geometry.

The total reconstruction time can be split into two parts: a *preprocessing time*, where the filters are calculated once for a given geometry, and a *reconstruction time*, where the actual reconstruction method is applied. The preprocessing time depends on the parameters that are used. For lNN-FBP, this step consists of the training stage and depends on both the geometry and the size of the training set. For AF-FBP the preprocessing time depends on the algebraic method that is used

and the geometry. The method OFBP requires only a small amount of preprocessing time compared to AF-FBP and lNN-FBP. The other methods do not require processing time or they calculate a filter based on the projection data of the scanned object. The time required for these calculations is included in the reconstruction time. Therefore, the reconstruction time of MR-FBP is high compared to that of the other methods.

The last three characteristics concern additional elements that are required for the preprocessing step. The method lNN-FBP requires a training set to be able to compute the filter, OFBP requires a phantom (in 3D three thin rods) to calculate the filter, and filters from MR-FBP depend on the scanned object.

7.3 EXPERIMENTS

In this section we describe the experiments that were performed and the choices that were made to implement the reconstruction methods. We compare the reconstruction time and preprocessing time of the different reconstruction methods. We also compare the quality of the reconstructions with the phantom using both the mean square error (MSE) and the structural similarity index (SSIM) for varying numbers of projection angles and for varying amounts of Poisson noise (expressed by the detector count I_0).

7.3.1 *Phantoms*

The Shepp-Logan phantom is used in the first series of experiments. It consists of a well-described pattern of ellipses and gray values, see Fig. 7.1a.

In the second series of experiments a foam phantom is used which is obtained from experimental micro-CT data, see Fig. 7.1b. The original cone beam dataset was obtained by a Skyscan 1172 with 511 projection angles. The reconstructed foam is a 3D object of consisting of 524 2D slices of 1000×1000 pixels. A slice close to the center of the foam is used as the phantom for the experiments. Different slices from the 3D object are used as training examples for lNN-FBP.

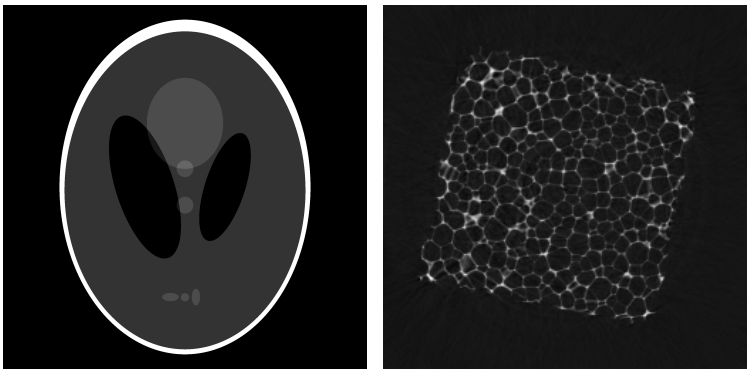

(a) Shepp-Logan (b) Metal foam

Figure 7.1: The phantoms.

7.3.2 *Implementation details*

The standard Ram-Lak filter for FBP is the windowed Ramp filter, where the window is the interval $[-1, 1]$. The same window is used for the Cosine and Hann filter, where some smoothening function is applied to Ram-Lak filter.

There are several implementation details to be discussed for the MR-FBP algorithm. The matrix W can be too large to obtain explicitly. Therefore, the matrix $\mathbf{A_p} = \boldsymbol{W}\boldsymbol{W}^{\mathsf{T}}\mathbf{C_p}$ is obtained column-by-column, where each column is obtained as the forward projection of applying FBP with unit vectors (with entries in $\{0, 1\}$) as filters to the projection data $\mathbf{p}$. Furthermore, exponential binning is used to reduce the number of unknowns for the filter $\mathbf{h}$. Small bins are used around the center of the detector, and the size of the bins increases exponentially further away from this center. The filter is also assumed to be symmetric around this center, which decreases the number of unknowns even further. The direct method called `gels*` lapack routine is used to find $\mathbf{h}^*$ in Eq. (7.10).

For the AF-FBP method the algebraic reconstruction method SIRT with $k = 100$ iterations and relaxation parameter $\omega = 1$ is used to obtain the filters. The method SIRT itself is also included in the experimental results to give an idea of the reconstruction time and accuracy of an algebraic method.

For the method of Zeng there are two parameters to be chosen in advance. Zeng has empirically determined the value of the relaxation parameter $\omega = 0.5$ for the filter function to be the optimal value. The number of iterations k of the Landweber algorithm is chosen to be $k = 100$.

The method OFBP is described for breast tomosynthesis. Since there are no limitations that prevent applying it to other geometries, we will apply it in this chapter to the parallel beam geometry. Instead of a thin rod we use a thin line placed vertically through the center of the detector as a 2D-phantom to calculate the filters. The thickness of the line equals the size of a detector pixel. Supersampling of 25 beams per detector pixel is used to obtain the projections. The number of iterations used for P-SIRT is $k = 10$ and the relaxation parameter for P-SIRT is $\omega = 1$. It will become clear in the results section that $k = 10$ is not always the optimal choice. We therefore also include some results with $k = 100$, which is the same number of iterations that is used for AF-FBP and Zeng, even though it is outside the scope of this work to determine (near) optimal parameters for every filter method.

The set of training objects for lNN-FBP consists of 100 slightly altered Shepp-Logan phantoms, where either the direction of some ellipses, or the size or gray value is altered. Every image pixel of the training object can be used to train the neural network. Therefore, the size of the total training set is much higher than the number of training objects. The total training set and the validation set consist each of 10^6 different image pixels. We use the Levenberg-Marquardt algorithm to find the vectors q_0^* and $\hat{h}_0^*$ that minimize the square differences between the output of the multilayer perceptron and the correct output. Furthermore, we use the Nguyen-Widrow initialization method to obtain start values for the parameters. Lastly, exponential binning is implemented to reduce the training time.

7.3.3 *Geometry parameters*

As mentioned before, a parallel beam scanning geometry has been used to obtain the projection data. The weight of each image projection for a specific projection is determined using the Joseph kernel. The number of projection angles N_Θ varies between 8 and 64 and the projection angles are sampled equiangularly in the interval $[0, 180)$ de-

grees. The number of counts on the detector I_0 is varied from 10^3 (high noise level) to 10^6 (low noise level).

The projection data is downsampled to 256 bins and the phantoms are reconstructed on a square grid of 256×256 pixels. The phantom is also downsamples to 256×256 pixels and the reconstructions are compared with this downsampled phantom to avoid the inverse crime.

7.4 RESULTS

The results of the experiments will be presented in this section. We first give examples of filters for the different reconstruction methods. Then we compare the timings and we conclude this section with a comparison of the reconstruction qualities of the filtering methods.

7.4.1 *Filters*

The filters that are used in FBP vary per reconstruction method. They are all shown in Fig. 7.2 with $|\Theta| = 24$. If a filter is angle-dependent then the filter corresponding to an angle of 22.5 degrees is shown.

Note the difference in both the absolute values of the filter and in smoothening of the edge of the filter, which is mainly seen for FBP-Cos and FBP-Hann. Furthermore, we observe a local maximum between detector bins 1 and 50 in the experimentally determined filters MR-FBP, SIRT-FBP, OFBP and lNN-FBP. This local maximum is not present in the theoretically derived filters FPB-RL, FBP-Cos, FBP-Hann and Zeng.

We also notice the small filter values for OFBP with 10 iterations, the number of iterations that was suggested by the inventors [8]. When we compare the reconstruction qualities of the different methods, then OFBP with $k = 10$ is not competitive with the other methods. We therefore adjusted the number of iterations to $k = 100$, which is the same number of iterations as for SIRT-FBP and Zeng. The impact of this decision is shown in Fig. 7.3 and Fig. 7.4, where the filters with $k = 10$ and $k = 100$ are shown corresponding to an angle of 22.5 degrees, and two reconstructions of the metal foam phantom are shown with $I_0 = 10^3$ and $|\Theta| = 64$. Also note the resemblance of the filters between OFBP with $k = 100$ and SIRT-FBP with $k = 100$. Since the filters for $k = 100$ substantially improve the results of OFBP, we have decided to show

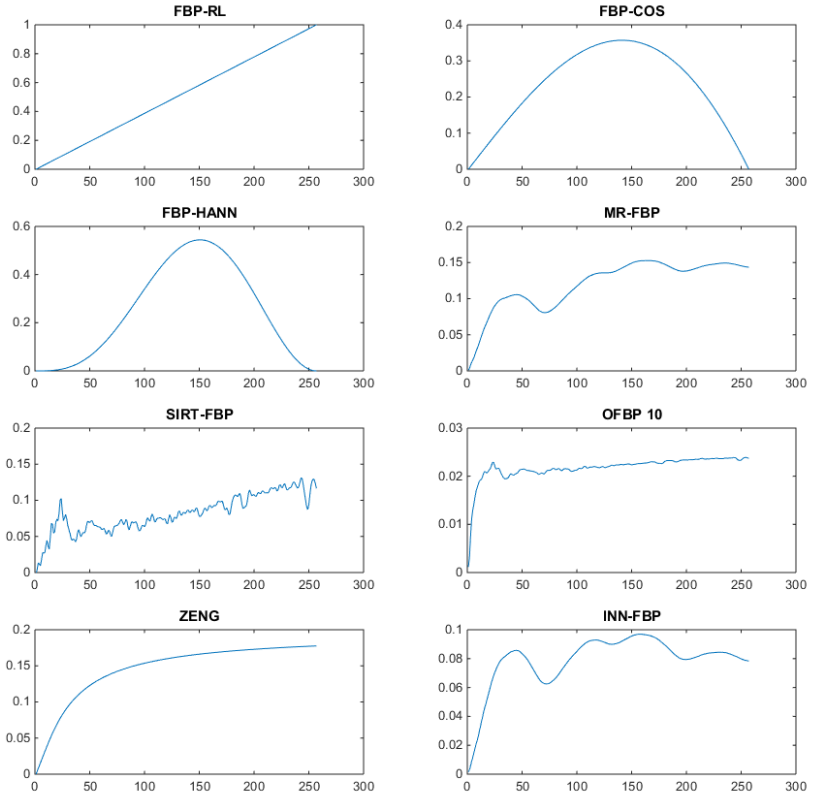

Figure 7.2: Filters for FBP with $|\Theta| = 24$. The Shepp-Logan phantom is used for the MR-FBP filter calculation and for the training set for lNN-FBP.

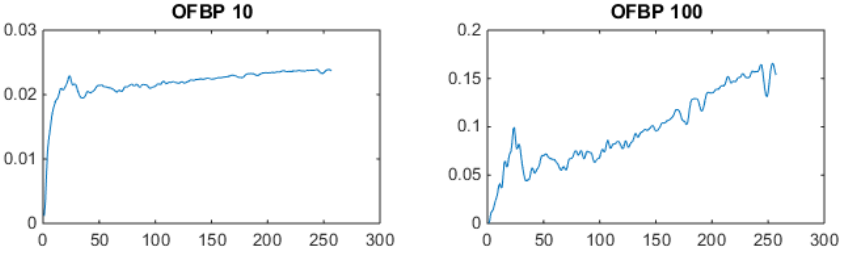

Figure 7.3: Filters for FBP with $|\Theta| = 24$ with $k = 10$ and $k = 100$, respectively.

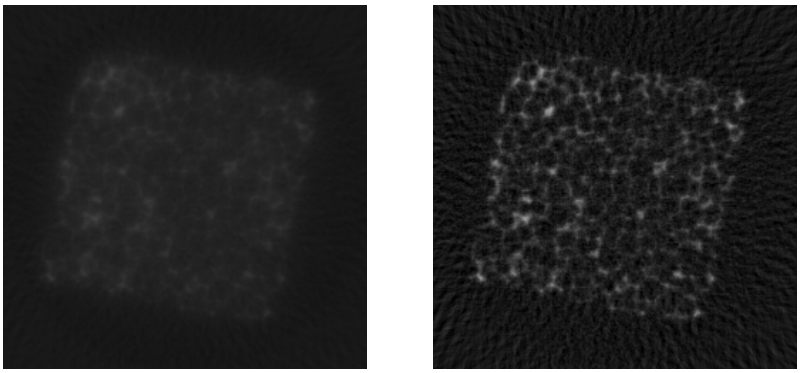

(a) (b)

Figure 7.4: Reconstructions of the metal foam phantom with $|\Theta| = 64$ and $I_0 = 10^3$ for OFBP with (a) $k = 10$, (b) $k = 100$.

Method	FBP-RL	FBP-Cos	FBP-Hann	MR-FBP	AF-FBP	Zeng	OFBP	lNN-FBP
PREP (s), $N_\Theta = 8$	$< 10^{-5}$	$< 10^{-5}$	$< 10^{-5}$	$1.8 * 10^{-3}$	55	$1.2 * 10^{-4}$	$2.8 * 10^{-1}$	300
PREP (s), $N_\Theta = 64$	$< 10^{-5}$	$< 10^{-5}$	$< 10^{-5}$	$2.2 * 10^{-3}$	775	$1.3 * 10^{-4}$	$8.3 * 10^{-1}$	295
REC ($*10^{-3}$ s), $N_\Theta = 8$	2.3	2.3	2.3	25	2.3	2.3	2.3	2.9
REC ($*10^{-3}$ s), $N_\Theta = 64$	3.6	3.7	3.7	43	3.7	3.7	3.7	4.3

Table 7.2: Preprocessing time (PREP) and reconstruction time (REC) for both $N_\Theta = 8$ and $N_\Theta = 64$ using the Shepp-Logan phantom with $I_0 = 5 * 10^3$.

results for OFBP with $k = 100$ in the remainder of this chapter, for reasons of better comparison. It is, however, not in any way the purpose of this work to find optimal parameters for the different reconstruction methods. We therefore use the parameters that are suggested by their inventors for the other reconstruction methods.

7.4.2 *Timings*

The time that is required to produce a reconstruction is split into the preprocessing time and the actual reconstruction time, see Section 7.2.8.

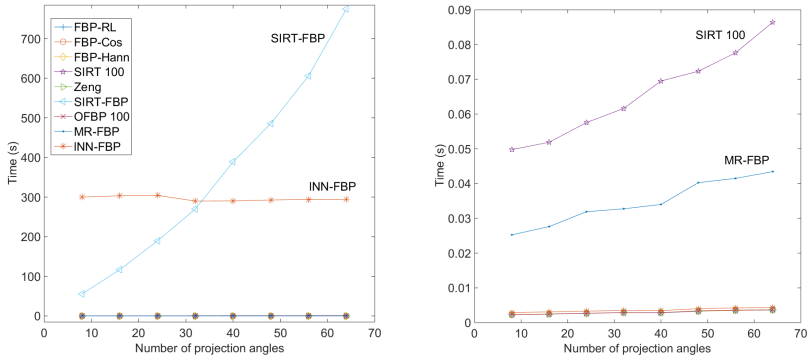

(a) Preprocessing time (b) Reconstruction time

Figure 7.5: Timings required to reconstruct the Shepp-Logan phantom.

The preprocessing times and reconstruction times for the different reconstruction methods are shown in Fig. 7.5 and Table 7.2 for $N_\Theta = 8$ and $N_\Theta = 64$ where $I_0 = 5 * 10^3$. The phantom to be reconstructed was the Shepp-Logan phantom.

We observe that the preparation time of lNN-FBP is substantial but does not increase with increasing number of projection angles. The time that is required to obtain a filter for SIRT-FBP increases linearly with the number of projection angles. The actual reconstruction time for these methods is comparable to that of FBP with standard filters, since no additional calculations need to be done after the filters have been created for a given geometry. In contrast to these methods, MR-FBP needs no preprocessing time, while the reconstruction time is substantially higher and increases with the number of projection angles. We have included the reconstruction time that is required for SIRT with $k = 100$ iterations for comparison.

We also observe a slightly larger reconstruction time for lNN-FBP compared to for example FBP with standard filters. The difference is small though, and is due to a slightly different implementation.

7.4.3 *Number of projection angles*

In this series of experiments, we vary the number of projection angles and show the resulting MSE and SSIM for a fixed amount of noise

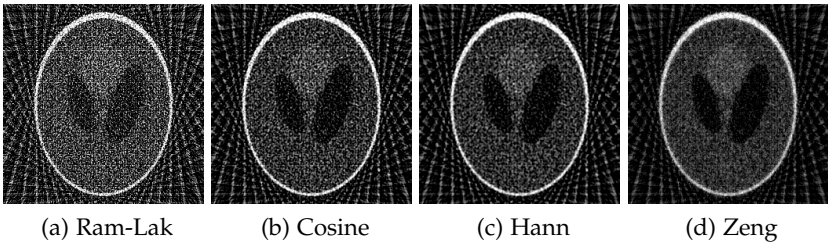

(a) Ram-Lak (b) Cosine (c) Hann (d) Zeng

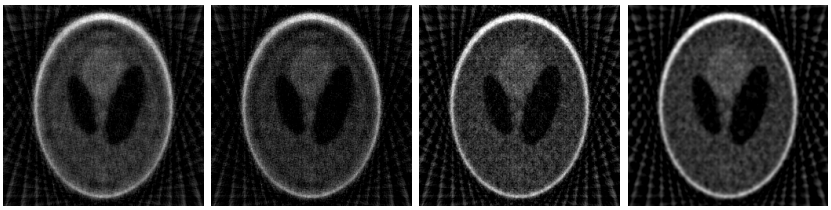

(e) SIRT-FBP (f) OFBP 100 (g) MR-FBP (h) lNN-FBP

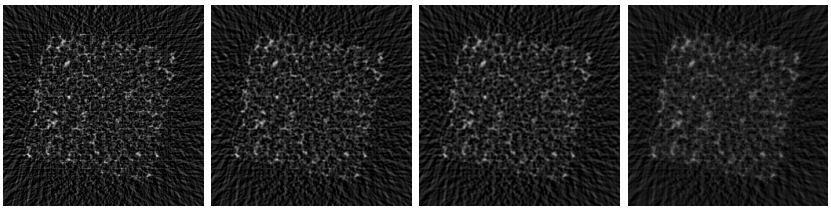

(i) Ram-Lak (j) Cosine (k) Hann (l) Zeng

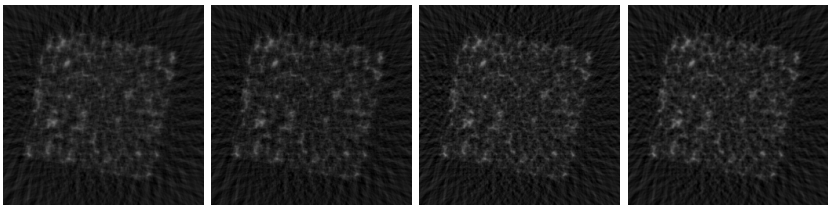

(m) SIRT-FBP (n) OFBP 100 (o) MR-FBP (p) lNN-FBP

Figure 7.6: Reconstructions of (a)-(h) the Shepp-Logan phantom, $I_0 = 10^3$, $|\Theta| = 24$, (i)-(p) the metal foam phantom, $I_0 = 10^4$, $|\Theta| = 32$.

applied to the projection data. We first show some reconstructions in Fig. 7.6 of the Shepp-Logan phantom for $I_0 = 10^3$ and $|\Theta| = 24$, and of the metal foam for $I_0 = 10^4$ and $|\Theta| = 32$. The results for both the Shepp-Logan phantom and the metal foam phantom with $I_0 = 10^3$ are shown in Fig. 7.7.

We observe that the differences in performance with this high noise level are large for both the MSE and SSIM measure. For few projection angles, FBP with standard filters and the method of Zeng are clearly outperformed by the other methods. FBP with the Ram-Lak filter performs worst with respect to both measures for all considered projection data. For a larger number of projection angles, the differences in reconstruction quality become smaller.

The reconstruction methods lNN-FBP, SIRT-FBP, SIRT and OFBP perform similarly with respect to both the MSE and SSIM, where we note that lNN-FBP is slightly better than the other methods. The exception is the SSIM for the Shepp-Logan phantom, where lNN-FBP is substantially more accurate than all other filter methods. Furthermore, we observe that the reconstruction quality of SIRT-FBP and SIRT is comparable, and that it is slightly better than OFBP with respect to the MSE. For a sufficiently large number of projection angles, the SSIM of OFBP is larger than that of SIRT-FBP.

The reconstruction quality of MR-FBP for low numbers of projection angles is relatively high compared to the other methods, while for higher numbers of projection angles MR-FBP performs relatively poorly.

7.4.4 *Poisson noise*

For the second series of experiments, we vary the amount of Poisson noise for a fixed number of projection angles. Again we observe that the reconstruction quality strongly depends on the chosen parameters, the phantom that is used and on the number of projection angles. This is demonstrated in Fig. 7.8, where the MSE and SSIM are shown for reconstructions of the Shepp-Logan phantom and the metal foam phantom for both $|\Theta| = 16$ and $|\Theta| = 64$.

For few projection angles, the standard filters Ram-Lak, Cosine and Hann are outperformed by the other methods. Also Zeng cannot compete with the other filter methods for the metal foam phantom. For the Shepp-Logan phantom, however, the method of Zeng is a strong

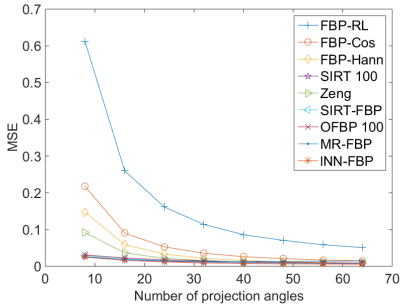

(a) Shepp-Logan

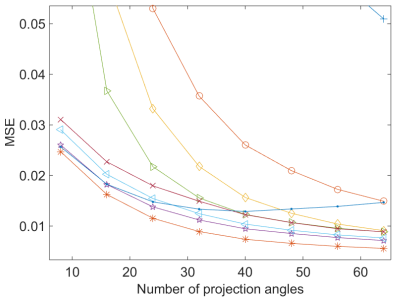

(b) Shepp-Logan, detail

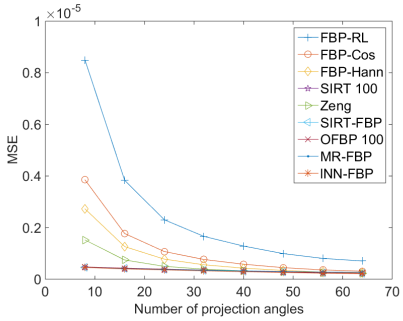

(c) Metal foam

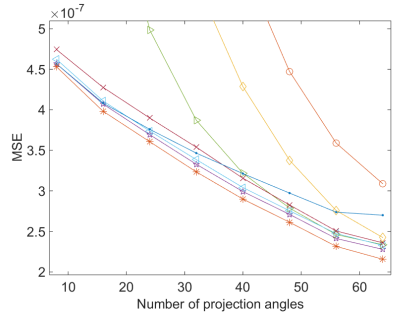

(d) Metal foam, detail

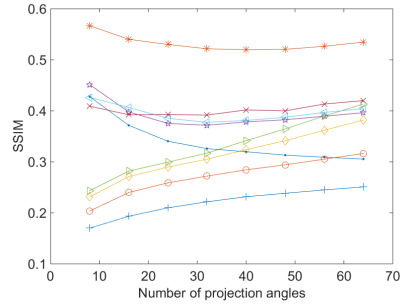

(e) Shepp-Logan

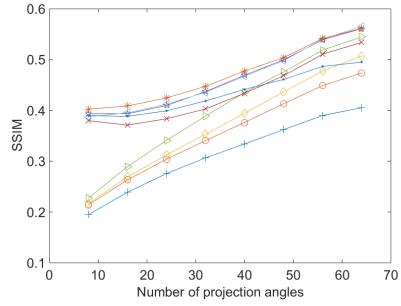

(f) Metal foam

Figure 7.7: Mean square error and structural similarity index measure with $I_0 = 10^3$.

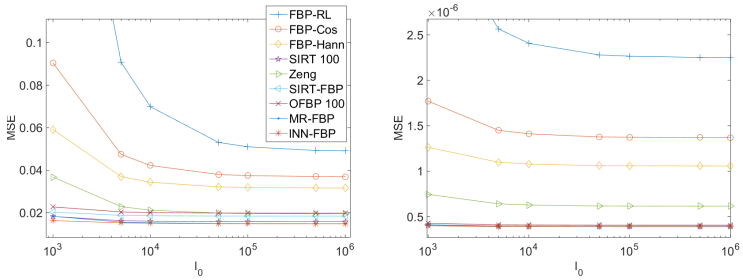

(a) Shepp-Logan, $|\Theta| = 16$ (b) Metal foam, $|\Theta| = 16$

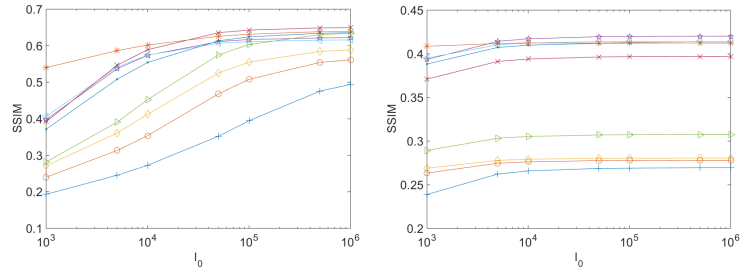

(c) Shepp-Logan, $|\Theta| = 16$ (d) Metal foam, $|\Theta| = 16$

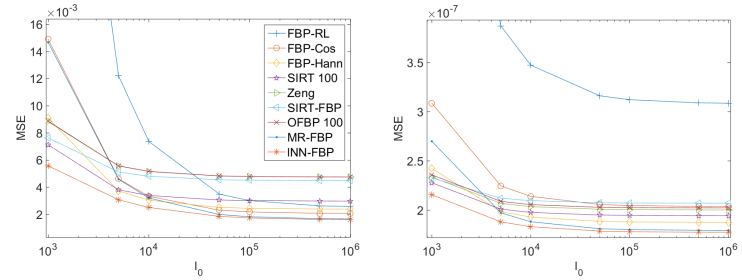

(e) Shepp-Logan, $|\Theta| = 64$ (f) Metal foam, $|\Theta| = 64$

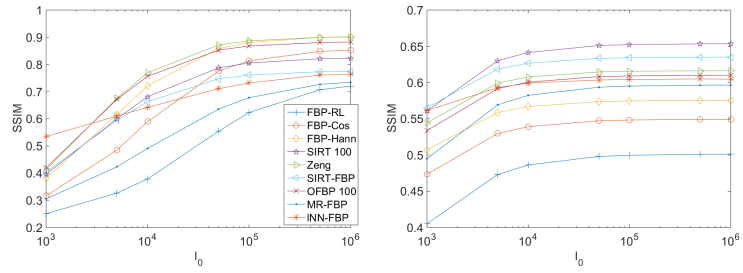

(g) Shepp-Logan, $|\Theta| = 64$ (h) Metal foam, $|\Theta| = 64$

Figure 7.8: Quality of the reconstructions using the MSE and SSIM.

competitor for the other methods. The ranking of these methods also depends on the measure; for MSE the method lNN-FBP performs best for both phantoms, while for SSIM the outcome does not only depend on the phantom, it also depends on the amount of noise that is applied to the projection data. The methods lNN-FBP, OFBP and SIRT all perform best for a specific combination of these influencing factors.

The results also depend heavily on the number of projection angles. For the high number of projections $|\Theta| = 64$, we observe that lNN-FBP performs very well with respect to the MSE, while the SSIM of lNN-FBP varies from the best to below average compared to the other methods. The opposite is seen for SIRT-FBP, OFBP and Zeng, where for example the MSE of SIRT-FBP is large for low noise levels, while the SSIM varies from the best to average depending on the phantom that is reconstructed. The method MR-FBP performs well with respect to the MSE for low noise levels, while it ranges from poorly to average for the SSIM.

7.5 DISCUSSION AND CONCLUSIONS

The scientific research of the last decade that had aimed at improving filters for FBP has resulted in several new filtering methods. In this chapter we presented an overview of these algorithms and compared their characteristics. We have also shown some reconstruction results for two different phantoms.

Since the reconstruction methods have very different characteristics, the choice for a specific reconstruction method depends on many factors. Time constraints are often an important factor in this decision; in this work both the preprocessing time and the reconstruction time are considered during the experiments. Furthermore, the number of projection angles and the amount of noise have a large impact on the quality of the reconstructions. Some filtering methods are better at handling few projection angles and high noise levels than others. Another factor that can play a role in the choice for a specific reconstruction method is the ability to incorporate prior knowledge.

The reconstruction methods lNN-FBP and AF-FBP require a large amount of preprocessing time and are therefore only suitable if the filters can be repeatedly used in a large number of experiments. The method OFBP also requires some preprocessing time, but this is small com-

pared to AF-FBP. The method MR-FBP requires a large reconstruction time, since it calculates a filter for every reconstruction based on the measured projections. Therefore this method is less favorable if large numbers of objects need to be scanned. The theoretically derived filters Ram-Lak, Cosine, Hann and Zeng require no preprocessing time and only a very short reconstruction time.

When not the reconstruction time but the ability to handle noise and few projection angles is the highest contributing factor to the choice for a reconstruction method, then the decision which method is best is less straightforward. We have shown that the reconstruction quality of the various methods depends highly on the number of projection angles and the amount of noise that is applied to the projection data. The suitability of the different methods varies with the phantom that is used. Furthermore, the outcome of comparing the reconstruction qualities depends on the choice of the measure. For the combination of geometry and phantoms we have considered here, the method lNN-FBP performs in most situations for both measures very well, while Ram-Lak, Cosine, Hann and Zeng cannot handle few projection angles and high noise levels well. The relative reconstruction qualities of the methods AF-FBP, MR-FBP and OFBP vary too much per phantom and geometry to draw any conclusions on which one performs best.

The ability to incorporate some types of prior knowledge is not examined in this chapter. Neither did we attempt to optimize the parameters of the reconstruction methods, such as the number of iterations k or the relaxation parameter ω. We have used the values suggested by their inventors, with the exception of OFBP since its reconstruction quality was otherwise not competitive with respect to the other filtering methods. Optimizing the parameters is outside the scope of this work.

Furthermore, we have deliberately refrained ourselves from any attempt to explain the observations in the Results section. Instead, we have limited our comments to a description of the behavior of the filtering methods. Since the aim of this chapter is to give an overview of the different filtering methods and their characteristics, the Results section is merely an illustration of the preceding theory. It requires further research with an increased number of phantoms and varying scanning geometries to be able to recommend filtering methods for specific reconstruction settings.

BIBLIOGRAPHY

[1] S. Van Aert et al. Three-dimensional atomic imaging of crystalline nanoparticles. *Nature* 2011; 470(7334): 374–377.

[2] T. M. Buzug. *Computed Tomography: From Photon Statistics to Modern Cone-Beam CT*. Berlin: Springer, 2008.

[3] H. Sipila. Moving object computer-tomography for luggage inspection. *Applications of Signal and Image Processing in Explosives Detection Systems*. Ed. by M. C. Connelly and S. M. Cheung. Proc. SPIE, 1993; 1824: 39–40.

[4] G. Nolet. *Seismic Tomography: With Applications in Global Seismology and Exploration Geophysics*. Dordrecht: Springer Netherlands, 1987.

[5] G. T. Herman. *Fundamentals of Computerized Tomography: Image Reconstruction from Projections*. Berlin: Springer, 2009.

[6] F. Natterer. *Mathematical methods in image reconstruction*. Philadelphia: SIAM, 2001.

[7] G. L. Zeng. A filtered backprojection algorithm with characteristics of the iterative Landweber algorithm. *Med. Phys.* 2012; 39(2): 603–607.

[8] H. Kunze et al. Filter determination for Tomosynthesis aided by iterative reconstruction techniques. *Proc. of Fully3D* 2007: 309–312.

[9] K. J. Batenburg and L. Plantagie. Fast Approximation of Algebraic Reconstruction Methods for Tomography. *IEEE Trans. Image Process.* 2012; 21(8): 3648–3658.

[10] D. M. Pelt and K. J. Batenburg. Fast tomographic reconstruction from limited data using artificial neural networks. *IEEE Trans. Image Process.* 2013; 22(12): 5238–5251.

[11] D. M. Pelt and K. J. Batenburg. Improving Filtered Backprojection Reconstruction by Data-Dependent Filtering. *IEEE Trans. Image Process.* 2014; 23(11): 4750–4762.

[12] D. J. Godfrey, H. P. McAdams, and J. T. Dobbins 3rd. Optimization of the matrix inversion tomosynthesis (MITS) impulse response and modulation transfer function characteristics for chest imaging. *Med Phys.* 2006; 33(3): 655–667.

[13] T. Nielsen et al. Filter Calculation for X-Ray Tomosynthesis Reconstruction. *Phys. Med. Biol* 2012; 57(12): 3915–3930.

[14] A. C. Kak and M. Slaney. *Principles of Computerized Tomographic Imaging*. Philadelphia: SIAM, 2001.